

A pan-cancer PDX histology image repository with genomic and pathological annotations for deep learning analysis

Brian S White*, The Jackson Laboratory for Genomic Medicine
Xing Yi Woo*, The Jackson Laboratory for Genomic Medicine
Soner Koc*, Seven Bridges Genomics, Inc
Todd Sheridan, The Jackson Laboratory for Genomic Medicine
Steven B Neuhauser, The Jackson Laboratory
Shidan Wang, University of Texas Southwestern Medical Center
Yvonne A Evrard, Leidos Biomedical Research Inc., Frederick National Laboratory for Cancer Research
John David Landua, Baylor College of Medicine
R Jay Mashl, Washington University School of Medicine
Sherri R Davies, Washington University School of Medicine
Bingliang Fang, The University of Texas MD Anderson Cancer Center
Maria Gabriela Raso, The University of Texas MD Anderson Cancer Center
Kurt W Evans, The University of Texas MD Anderson Cancer Center
Matthew H Bailey, Simmons Center for Cancer Research, Brigham Young University
Yeqing Chen, The Wistar Institute
Min Xiao, The Wistar Institute
Jill Rubinstein, The Jackson Laboratory for Genomic Medicine
Ali Foroughi pour, The Jackson Laboratory for Genomic Medicine
Lacey Elizabeth Dobrolecki, Baylor College of Medicine
Maihi Fujita, Huntsman Cancer Institute, University of Utah
Junya Fujimoto, The University of Texas MD Anderson Cancer Center
Guanghua Xiao, University of Texas Southwestern Medical Center
Ryan C Fields, Washington University School of Medicine
Jacqueline L Mudd, Washington University School of Medicine
Xiaowei Xu, The Wistar Institute
Melinda G Hollingshead, National Cancer Institute
Shahanawaz Jiwani, Leidos Biomedical Research Inc., Frederick National Laboratory for Cancer Research
PDXNet consortium
Brandi Davis-Dusenberry, Seven Bridges Genomics, Inc
Tiffany A Wallace, National Cancer Institute
Jeffrey A Moscow, National Cancer Institute
James H Doroshow, National Cancer Institute
Nicholas Mitsiades, Baylor College of Medicine
Salma Kaochar, Baylor College of Medicine
Chong-xian Pan, University of California - Davis
Moon S Chen Jr, University of California - Davis
Luis G Carvajal-Carmona, University of California - Davis
Alana L Welm, Huntsman Cancer Institute, University of Utah
Bryan E Welm, Huntsman Cancer Institute, University of Utah

Ramaswamy Govindan, Washington University School of Medicine
Shunqiang Li, Washington University School of Medicine
Michael A Davies, The University of Texas MD Anderson Cancer Center
Jack A Roth, The University of Texas MD Anderson Cancer Center
Funda Meric-Bernstam, The University of Texas MD Anderson Cancer Center
Yang Xie, University of Texas Southwestern Medical Center
Meenhard Herlyn, The Wistar Institute
Li Ding, Washington University School of Medicine
Michael T Lewis, Baylor College of Medicine
Carol J Bult, The Jackson Laboratory
Dennis A Dean II, Seven Bridges Genomics, Inc
Jeffrey H Chuang, The Jackson Laboratory for Genomic Medicine

*: co-first authors

Abstract

Patient-derived xenografts (PDXs) model human intra-tumoral heterogeneity in the context of the intact tissue of immunocompromised mice. Histological imaging via hematoxylin and eosin (H&E) staining is performed on PDX samples for routine assessment and, in principle, captures the complex interplay between tumor and stromal cells. Deep learning (DL)-based analysis of large *human* H&E image repositories has extracted inter-cellular and morphological signals correlated with disease phenotype and therapeutic response. Here, we present an extensive, pan-cancer repository of nearly 1,000 *PDX* and paired human progenitor H&E images. These images, curated from the PDXNet consortium, are associated with genomic and transcriptomic data, clinical metadata, pathological assessment of cell composition, and, in several cases, detailed pathological annotation of tumor, stroma, and necrotic regions. We demonstrate that DL can be applied to these images to classify tumor regions and to predict xenograft-transplant lymphoproliferative disorder, the unintended outgrowth of human lymphocytes at the transplantation site. This repository enables PDX-specific, investigations of cancer biology through histopathological analysis and contributes important model system data that expand on existing human histology repositories. We expect the PDXNet Image Repository to be valuable for controlled digital pathology analysis, both for the evaluation of technical issues such as stain normalization and for development of novel computational methods based on spatial behaviors within cancer tissues.

Introduction

The high clinical failure rate of cancer therapies is often attributed to the lack of tumor heterogeneity in pre-clinical models (Tentler et al. 2012). This concern has motivated increased use of patient-derived xenografts (PDXs), in which a fresh human tumor biopsy is implanted subcutaneously or orthotopically in the flank of an immunodeficient mouse. If the implantation successfully establishes the model in the *P₀* mouse, the tumor can be passaged in future

generations (P_1 , P_2 , etc.). After being sufficiently expanded, the model may be used for pre-clinical drug trials and these have successfully predicted therapeutic outcome in patients (Pompili et al. 2016).

PDXs have been shown to recapitulate phenotypes of their human progenitors along other dimensions as well. For example, PDX expression profiles correlate with those of their progenitors (Petrillo et al. 2012; S. Li et al. 2013) and these can be stably maintained for at least five generations (X. Zhang et al. 2013). Similar consistency between PDX and human and across passages has been demonstrated for copy number alterations (Woo et al. 2021). Finally, PDXs retain the invasive histological phenotype of their matched progenitor, as reflected in staining with hematoxylin and eosin [H&E; (X. Zhang et al. 2013)].

This latter finding raises the intriguing possibility that recent successes applying deep learning (DL) for whole-slide (WSI) analysis of H&E images in *human* (Aeffner et al. 2019; Komura and Ishikawa 2018; Srinidhi, Ciga, and Martel 2021) will be applicable to PDXs, as well. DL-based analyses of human data are capable of predicting metastases (Ehteshami Bejnordi et al. 2017), gene mutations (Coudray et al. 2018) and expression (Coudray et al. 2018; Schmauch et al. 2020), survival (Kather et al. 2019), cancer types (Noorbakhsh et al. 2020), molecular (Sirinukunwattana et al. 2021), clinical (Rawat et al. 2020), and histological (J. Li et al. 2022) tumor subtypes, and response to both chemotherapy (Farahmand et al. 2022) and immune checkpoint inhibitors (Johannet et al. 2021), amongst many other phenotypes reviewed extensively elsewhere (Tran et al. 2021; van der Laak, Litjens, and Ciompi 2021; Bera et al. 2019). DL approaches can, in principle, assess the complexity of spatial interactions between cancer, stromal, and immune cells reflected in H&E images, thus moving beyond cancer cell-intrinsic, univariate gene biomarkers. For example, DL methods were able to associate tumor-infiltrating lymphocyte spatial structure with survival (Saltz et al. 2018), and differentiate breast tumor samples from benign breast biopsies based on stroma (Saltz et al. 2018; Ehteshami Bejnordi et al. 2018).

The explosive growth of DL-based applications in digital pathology has been made possible by extensive, public repositories of human H&E images, such as in TCGA, The Cancer Imaging Archive, and Imaging Data Commons. No similar resource exists for PDX images. Here, we describe a large-scale repository of >800 PDX and >100 matched patient tumor H&E images, along with expansive genomic, transcriptomic, clinical, and pathological annotations. The images were curated as part of the National Cancer Institute's PDX Development and Trial Centers Research Network program (PDXNet), aimed at collaborative development and pre-clinical testing of targeted therapeutic agents. Thumbnails and clinical metadata of the images, along with the raw genomic and transcriptomic data, are available on the PDXNet portal (Koc et al. 2022). The raw images are hosted on the Seven Bridges Cancer Genomics Cloud [CGC; www.cancergenomicscloud.org; (Lau et al. 2017)] and will soon be available on the Imaging Data Commons (Fedorov et al. 2021). We present several use cases applying DL for classification of PDX images. The repository should facilitate monitoring of potential divergence between a PDX and its human progenitor during passaging (Ben-David et al. 2017) and exploration of questions uniquely relevant to PDX models, including the impact of human cell

turnover within the xenografts (Blomme et al. 2018; Sanz et al. 2009; Gray et al. 2004). We expect this PDXNet Image Repository to be valuable for controlled digital pathology analysis and development of novel computational methods based on spatial behaviors within patient-derived cancer tissues.

Results

A pan-cancer, multi-institutional repository links histology images to clinical annotations, pathological assessments, and genomic and transcriptomic data.

The PDXNet repository consists of 810 H&E images from PDXs and 139 from their paired human progenitors. They represent 33 cancer types (**Fig. 1A**), including breast cancer (BC; a category encompassing ductal carcinoma *in situ*, lobular carcinoma *in situ*, invasive breast carcinoma, invasive lobular carcinoma, and breast cancer not otherwise specified; $n=134$), colon adenocarcinoma (COAD; $n=94$), pancreatic cancer (PDAC; $n=87$), lung adenocarcinoma (LUAD; $n=80$), melanoma (SKCM; $n=71$), and squamous cell lung cancer (LUSC; $n=67$). Images were generated at five PDX Development and Trial Centers (PDTCs) within PDXNet – Baylor College of Medicine (BCM), Huntsman Cancer Institute (HCI), MD Anderson Cancer Center (MDACC), The Wistar Institute (WISTAR), and Washington University in St Louis (WUSTL) – as well as at the NCI Patient-Derived Models Repository (PDMR) and The Jackson Laboratory (JAX).

Most PDX images are from early passages, with those from P0 ($n=158$), P1 ($n=295$), and P2 ($n=155$) predominating over those from later passages ($> P2$; $n=171$; **Fig. 1B**). 102 images from human progenitors have at least one paired PDX image, for a total of 306 such images. Of these, cancer diagnoses with images from at least four unique, paired progenitors include BC, COAD, LUSC, Non-Rhabdomyosarcoma soft tissue sarcomas (NRSTS; a category encompassing non-infantile fibrosarcoma, gastrointestinal stromal tumor, non-uterine leiomyosarcoma, malignant peripheral nerve sheath tumor, and synovial sarcoma), SKCM, and LUAD (**Fig. 1C**). The repository includes images from mice that were treated therapeutically, whose human progenitor was treated therapeutically, or that are completely treatment naïve. Diagnoses having at least two treated PDXs or PDXs derived from at least two treated progenitors include BC, COAD, PDAC, LUAD, SKCM, and colorectal cancer (CRC; **Fig. 1D**).

H&E images are linked to RNA-seq and whole exome sequencing (WES) data hosted on the PDXNet portal (Koc et al. 2022): 36 of 106 human progenitors, 98 of 289 PDX models, and 509 of 799 mice bearing PDXs are characterized by histological imaging, transcriptomically, and genetically (**Figs 1E-G**). Additionally, most images include pathological assessment of tumor stage ($n=650$) and slide-level proportions of cancer, stromal, and necrotic regions ($n=626$; **Fig. 1A**).

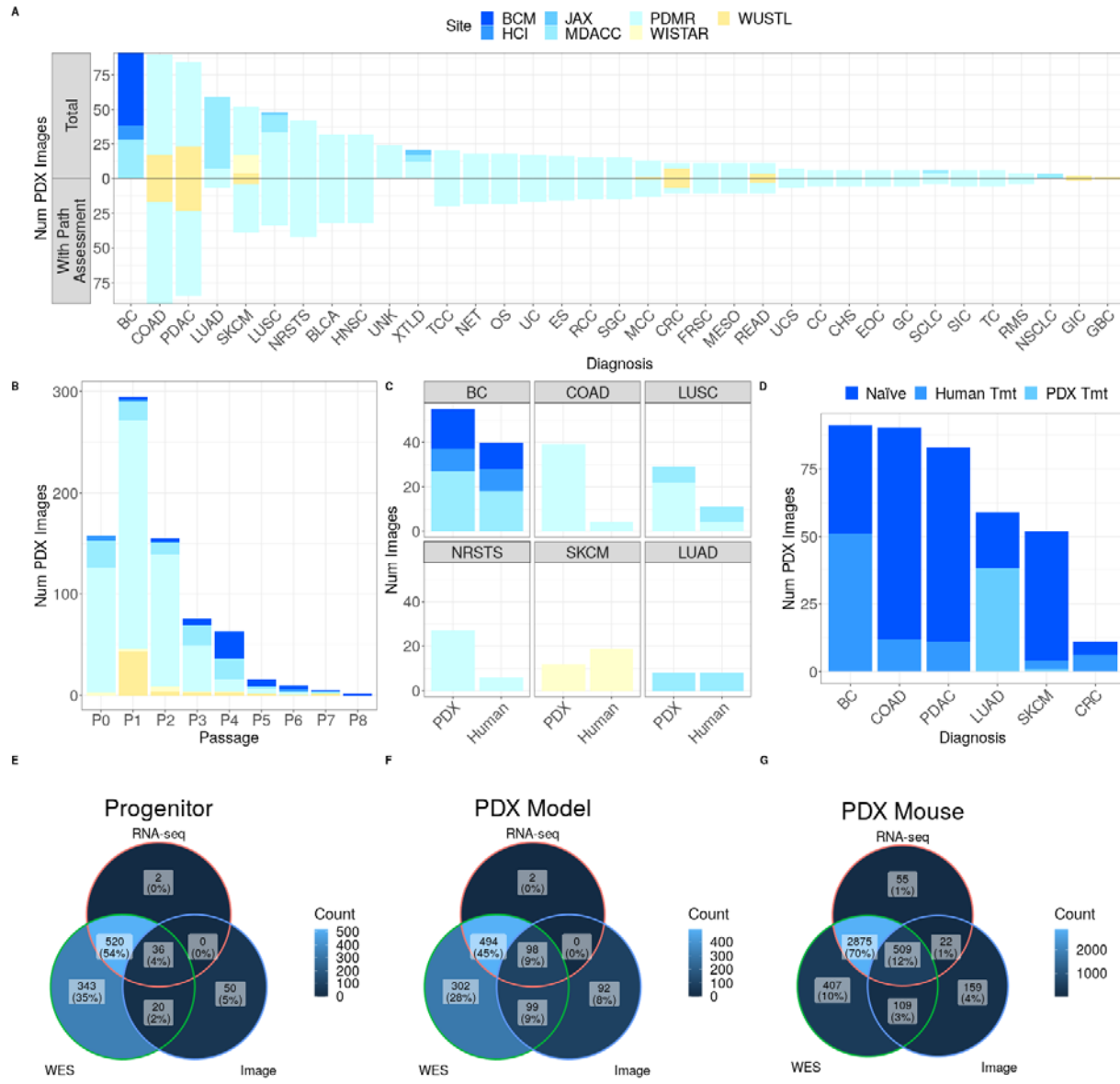


Fig 1. PDXNet Image Repository captures heterogeneity across tumor types, passages, and treatment status and pairs histology images with pathological assessment and genomic and transcriptomic data. (A) Distribution of total PDX H&E images and subset with pathological assessment by diagnosis. (B) Distribution of PDX images by passage. (C) Counts of images by source for those derived from human progenitor / PDX pairs, restricted to diagnoses with at least four such progenitors. (B, C) Barcharts colored according to contributing site as indicated in (A). (D) Distribution of PDX images across diagnoses with at least two treated PDXs or PDXs derived from at least two treated progenitors. (E, F, G) Intersection of image, RNA-seq, and WES data (E) amongst human progenitor samples, (F) across PDX models, and (G) across individual mice.

Pathologist cell type estimates allow evaluation of cell segmentation and classification.

We used pathologist estimates of percentage of neoplastic, stromal, and necrotic cells in *PDX* samples as ground truth in evaluating Hover-Net, a nuclei segmentation and classification trained on *human* H&E images (Graham et al. 2019). Hover-Net classifies nuclei as neoplastic, stromal (“connective”), necrotic, immune (“inflammatory”), non-neoplastic epithelial, and other. We derived a slide-level estimate for each cell type as the proportion of the corresponding nuclei area relative to the total tissue area (see Methods). Hover-Net-based slide-level estimates generally correlated well for neoplastic (median *weighted* Pearson correlation $r = 0.51$), stromal ($r = 0.52$), and necrotic ($r = 0.70$) cells across diagnoses (COAD, CRC, and PDAC) and datasets (PDMR and WUSTL; **Fig. 2**).

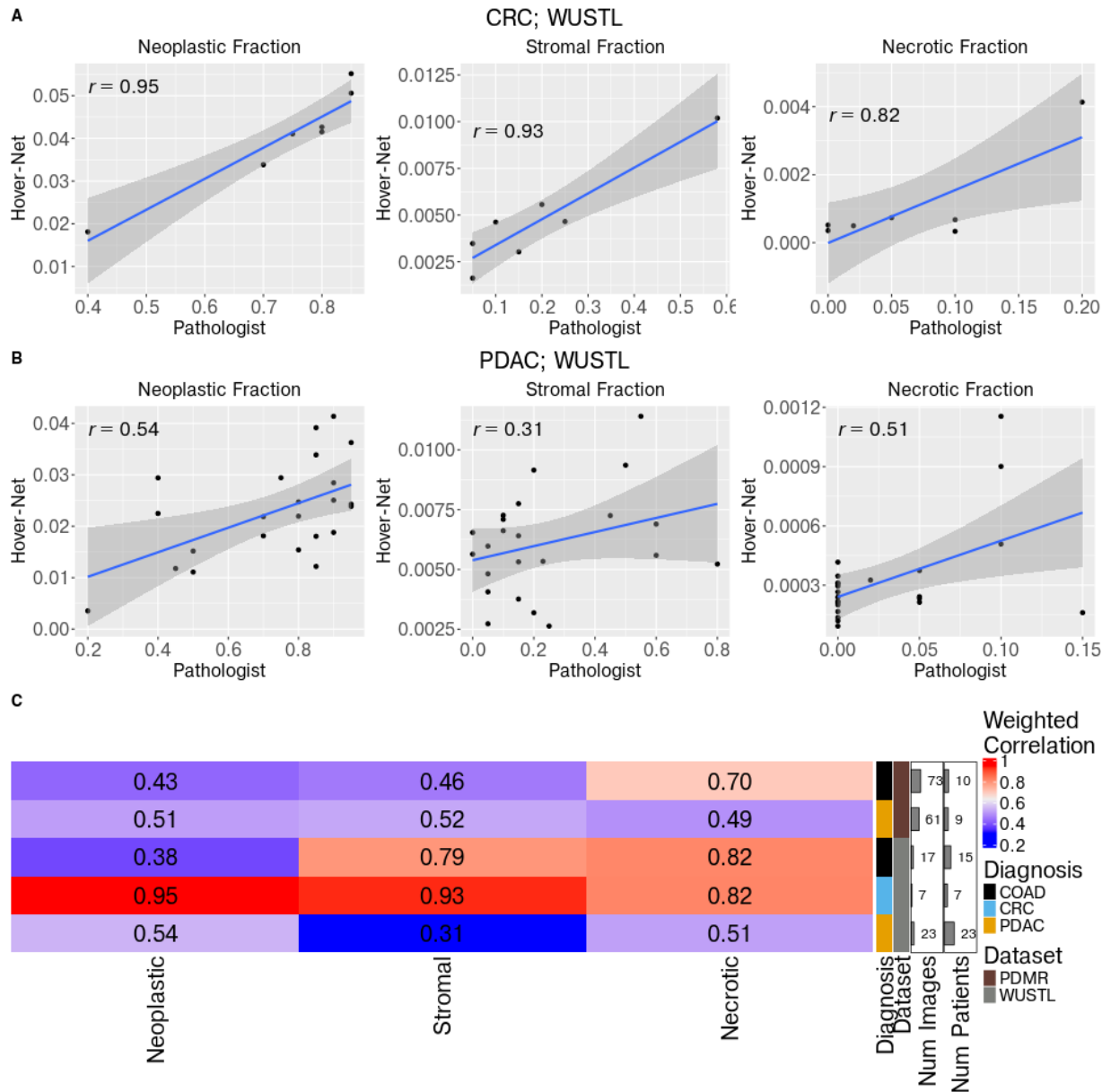
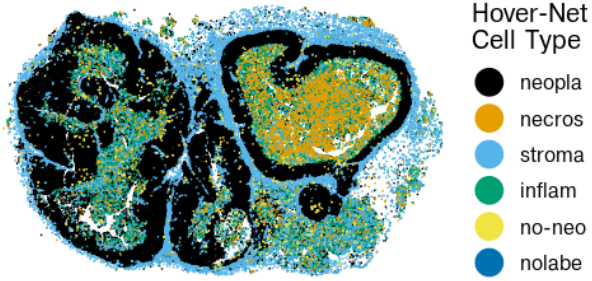


Fig 2. Cell segmentation and classification trained on human data correlate with pathologist estimates of cell type proportions in PDX samples. (A, B) Correlation of pathologist (x axis) and Hover-Net-based slide-level estimates (y axis) for neoplastic (left column), stromal (center column), and necrotic (right column) cell proportions in (A) CRC and (B) PDAC from WUSTL. Each point corresponds to an individual image and PDX (i.e., no replication). (C) Weighted Pearson correlations of pathologist and Hover-Net-based estimates of neoplastic, stromal, and necrotic cell proportions in COAD, CRC, and PDAC in the PDMR and WUSTL datasets. Correlations are computed over images, inversely weighted according to number of replicate images derived from the same patient. In cases without replication, the number of images equals the number of patients and weighted and unweighted Pearson correlation are identical.

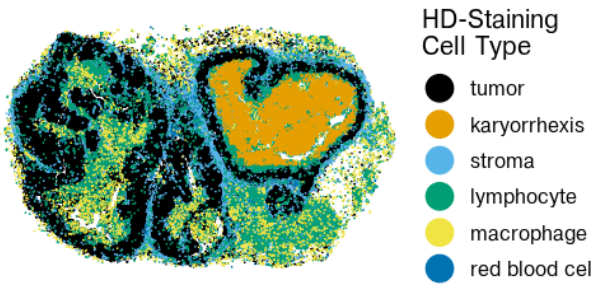
Pathologist pixel-level annotations enable training of a regional classifier.

To spatially contextualize slide-level correlations between predicted and assessed cell type proportions, a board-certified pathologist manually annotated cancer epithelium (“tumor”), stroma, and necrotic regions within H&E images of LUSC ($n=15$), LUAD ($n=18$), and BC ($n=8$; **Fig. 3E**). We labeled tiles according to their intersection with these annotations and found that, as expected, tumor tiles were predominantly composed of cells classified as neoplastic in the lung datasets (**Fig. S1**). Consistently, the spatial organization of predicted tumor cells closely resembled pathologist annotations (**Fig. 3A**). Breast cancer exhibited a different pattern, with most tiles composed of a mix of neoplastic and stromal cells. Lung stromal tiles harbored predicted neoplastic, immune, and stromal cells, whereas breast stromal tiles were predominantly comprised of stromal cells. Finally, necrotic tiles had levels of predicted necrotic cells in excess of those of other tiles in both tumor types, despite the additional presence of a larger proportion of neoplastic and immune cells in lung cancer and an appreciable proportion of stromal cells in breast cancer. To begin to address cellular heterogeneity within the stromal and necrotic regions, we applied a second nuclei segmentation and phenotyping approach, HD-Staining (S. Wang et al. 2020), to a PDX lung sample (**Fig. 3B**). The spatial pattern of HD-Staining phenotypes was broadly similar to that predicted by Hover-Net – though HD-Staining’s prediction of macrophages within one necrotic area was more fine-grained than the immune prediction of Hover-Net and the two disagreed about the immune content with one stromal region.

A



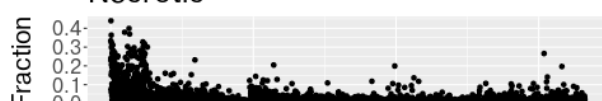
B



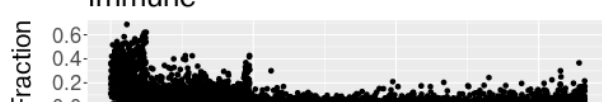
C Neoplastic



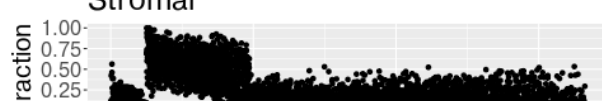
Necrotic



Immune

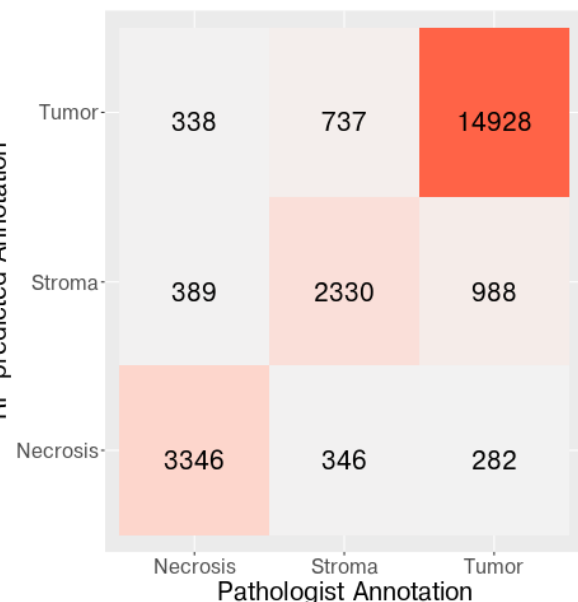


Stromal



Region ■ Stroma ■ Tumor ■ Necrosis

D



E

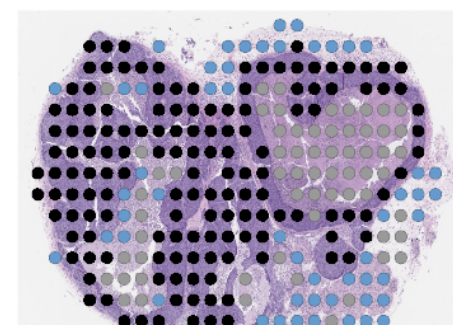
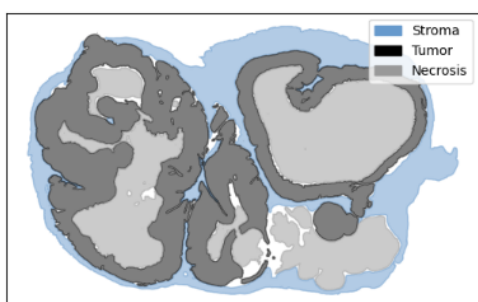


Fig 3. Regional classifier predicts cancer epithelium (“tumor”), stroma, and necrotic areas based on nuclei classification. (A, B) Cell phenotypes predicted by (A) Hover-Net or (B) HD-Staining within a PDX lung tumor. (C) Labeled tiles (columns; blue: stroma, black: tumor, gray: necrosis) represented according to the cellular fraction that is predicted by Hover-Net to be neoplastic, necrotic, immune, or stromal. (D) Confusion matrix comparing pathologist-provided tile labels with corresponding prediction from the RF Hover-Net classifier. (E) Pathologist regional annotations. (F) Random forest (RF) Hover-Net-based classifier predictions of regions (within 512 x 512 pixels).

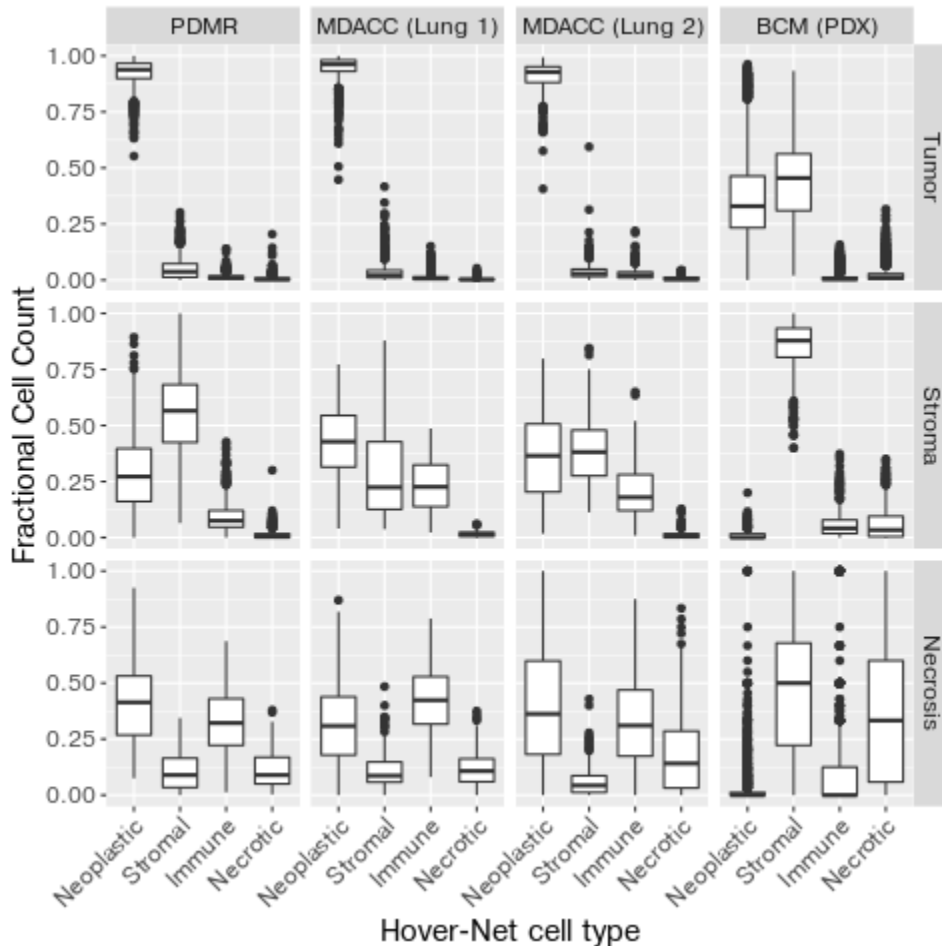


Fig S1. Regional proportions of cell types vary by cancer type. Boxplots show fraction of cells (y axis) of a particular type predicted by Hover-Net (x axis) relative to total number of segmented cells within a 512x512 pixel tile at 20X resolution. Results are stratified by dataset (columns) and pathologist-annotated region overlapping the tile (rows).

The localization of particular cell types within morphological regions has clinical implications. For example, tumor-stromal interactions have been associated with disease progression and

chemotherapy resistance in breast cancer (Farmer et al. 2009; Conklin and Keely 2012; Criscitiello, Esposito, and Curigliano 2014; “The Impact of Tumor Stroma on Drug Response in Breast Cancer” 2015; Plava et al. 2019). While regional annotations facilitate correlative studies with clinical phenotypes, the manual burden in generating them is high: a pathologist expended approximately 20 hours demarcating, in detail, regions within each sample.

To alleviate this annotation burden, we instead sought to predict tumor, stroma, and necrotic regions within H&E images. We first represented each tile according to the fraction (**Fig. 3C**) and count (**Fig. S2**) of each Hover-Net-predicted cell type within it. Consistent with our previous results, we observed that these tile profiles of constituent cell types were region- and cancer type-specific. We used the profiles as features and trained a random forest to (probabilistically) predict regions using them. Predictions correctly recapitulated irregular region boundaries (**Fig. 3F**) and performance was high (**Fig. 3D**; precision, recall, specificity, and accuracy all equal 0.87). Further, prediction performance was consistently high for all regions across cancer types, datasets, and individual samples: over tiles labeled as belonging to a particular region, the median probability of being assigned to that correct region was over 50% for the four samples in the lung PDMR dataset, for all but two of ten lung stromal regions and one of 12 tumor lung tumor regions in the MDACC dataset, and for all but one of seven breast tumor regions and one of five breast necrosis regions in the BCM dataset (**Fig. S3**).

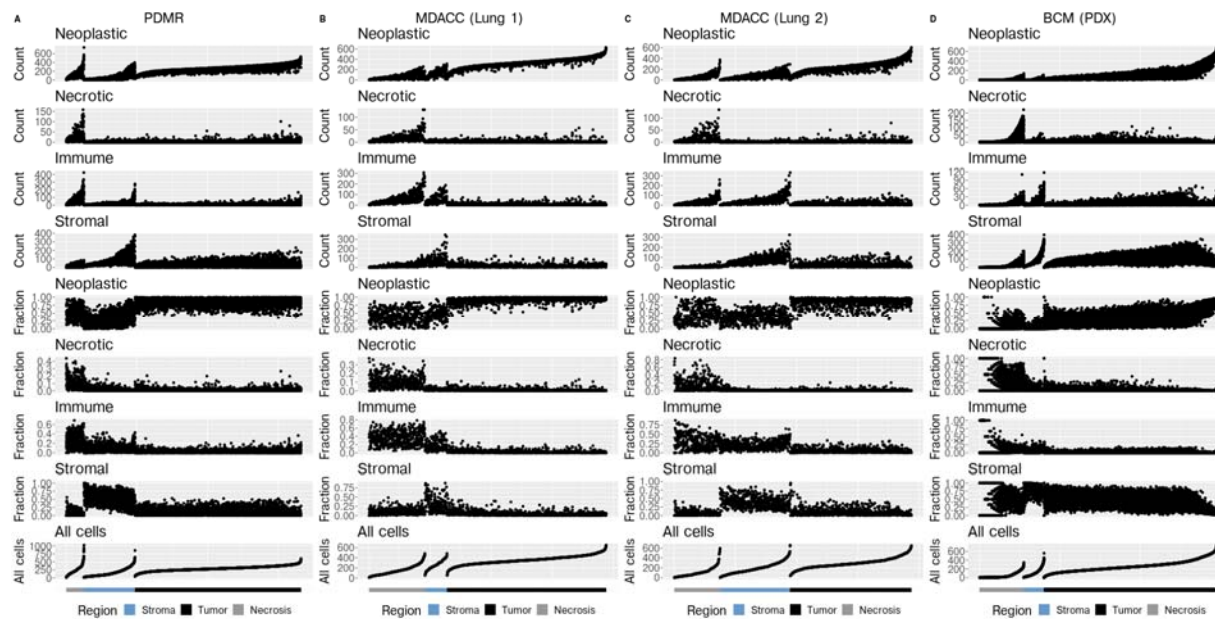


Fig S2. Regions have characteristic cell type proportions and counts that vary by cancer type. Each tile (columns within subpanels) is annotated according to region (tumor, stroma, or necrotic) and represented by the count and fractional proportion of each type of cell (neoplastic, necrotic, immune, or stromal) within it, as well as the total number of cells. Tiles are shown for lung cancer samples in the (A) PDMR and (B, C) two MDACC datasets and for breast cancer samples in the (D) BCM dataset.

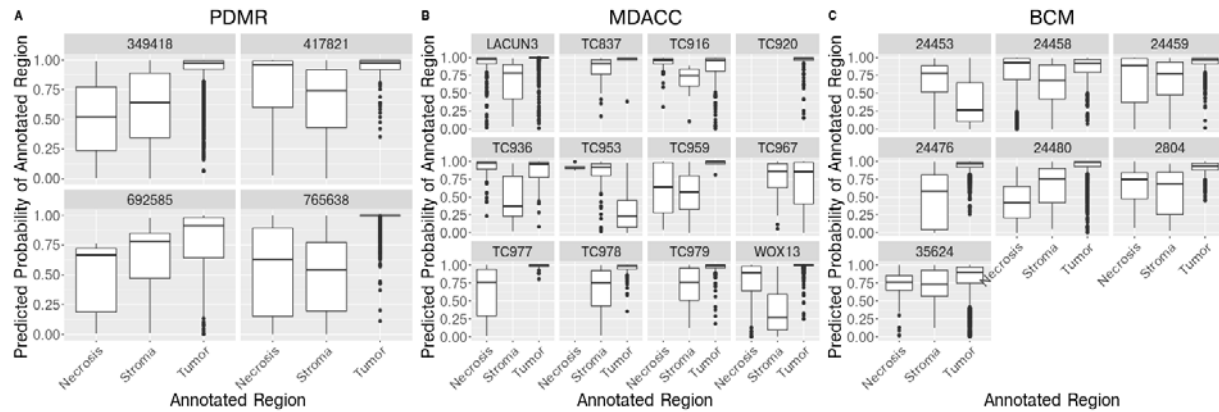


Fig S3. Regional classifier consistently and correctly predicts regions across cancer types, datasets, and samples. Boxplots show distribution over tiles of classifier-predicted probability that tile is assigned to the correct annotated region.

An H&E-based classifier identifies xenograft-transplant lymphoproliferative disorder.

During development of PDX models, human lymphocytes within the implanted tumor biopsy can overtake or limit the growth of the malignant cells. Such xenograft-transplant lymphoproliferative disorder (XTLD) is frequent, occurring at rates that exceed 10% in some transplanted cancer types (Butler et al. 2017; Bondarenko et al. 2015; Dieter et al. 2017; Choi et al. 2016) and that are variable across cancer types (L. Zhang et al. 2015). It can be detected during a quality control (QC) assessment of the generated model using immunohistochemistry (IHC) directed at human pan-immune (CD45) or B-cell (CD20) markers. It has also been detected and predicted based on expression differences between Epstein-Barr virus-associated lymphoma samples and non-lymphoma samples (Woo et al. 2019). Left undetected, however, XTLD would masquerade as the tumor type of the original biopsy, thus invalidating any downstream functional analysis or clinical correlation attempting to characterize that tumor type.

For labs that do not routinely perform IHC during a QC step and for legacy data without such an evaluation, we sought to develop an XTLD classifier applicable to H&E images generated during a standard pathological assessment. We reasoned that the higher density of small lymphocytes characteristic of XTLD (Fig. 4B) relative to an epithelial tumor (Fig. 4A) would be detectable via cell segmentation and classification. Indeed, we observed that the proportion of segmented immune cells was elevated in XTLD samples relative to LUSC samples in the MDACC ($p = 4.6 \times 10^{-4}$) and PDMR ($p = 0.08$) datasets (Fig. S4A). Further, median cell area (in 2D sections) of LUSC samples were higher than XTLD samples in MDACC and for all three of five LUSC samples in PDMR (Fig. S4B).

Despite the associations between XTLD and both immune cell proportion and cell size, the orderings induced by these two metrics imperfectly segregate XTLD and LUSC samples. Hence, we attempted a more general classification at the image tile level by representing each tile according to its cell classification-derived proportions of neoplastic, stromal, necrotic, and

immune cells, i.e., excluding the count-based features used in the regional classifier. We used these tile-level representations to train a random forest to predict XTLD status, similar to our approach above in predicting region labels. Tile-level prediction performance was strong (**Fig. 4D**), with precision, recall, specificity, accuracy, and AUC between 0.82 and 0.93 (**Fig. S5B, C**). Further, the distribution of tile-level XTLD probabilities were strongly skewed towards one for tiles from XTLD images and towards zero for those from LUSC images (**Fig. S5A**). As expected, immune proportions were more important than neoplastic and necrotic cell proportions and of similar importance to stromal cell proportions in predicting XTLD (**Fig. S6**). At the sample level, the Hover-Net-based classifier predicted the majority of tiles correctly (i.e., with probability > 0.5 for the annotated label) for 29 of 33 samples (**Fig. 4C**).

To improve upon sample level prediction, we next sought to generalize our classifier beyond its four biologically-inspired, but constrained, feature inputs. To do so, we extracted 2048 deep learning (DL) features from each tile using an Inception network v3 pre-trained on ImageNet (Szegedy et al. 2016; Noorbakhsh et al. 2020). These features were then input to a random forest classifier and the classifier was trained using the same assignment of tiles to folds as employed for the Hover-Net-based classifier. The Inception-based classifier improved performance over the Hover-Net-based model at both the tile-level (**Fig. 4F**), with precision, recall, specificity, accuracy, and AUC between 0.94 and 1.00 (**Fig. S5E, F**) and with a more pronounced skew of predicted probabilities towards their correct assignments (**Fig. S5D**), and at the sample-level, where 31 of 33 samples were predicted correctly (**Fig. 4E**). Additionally, the Inception-based model perfectly classified six samples in an external validation dataset (**Fig. 5A**).

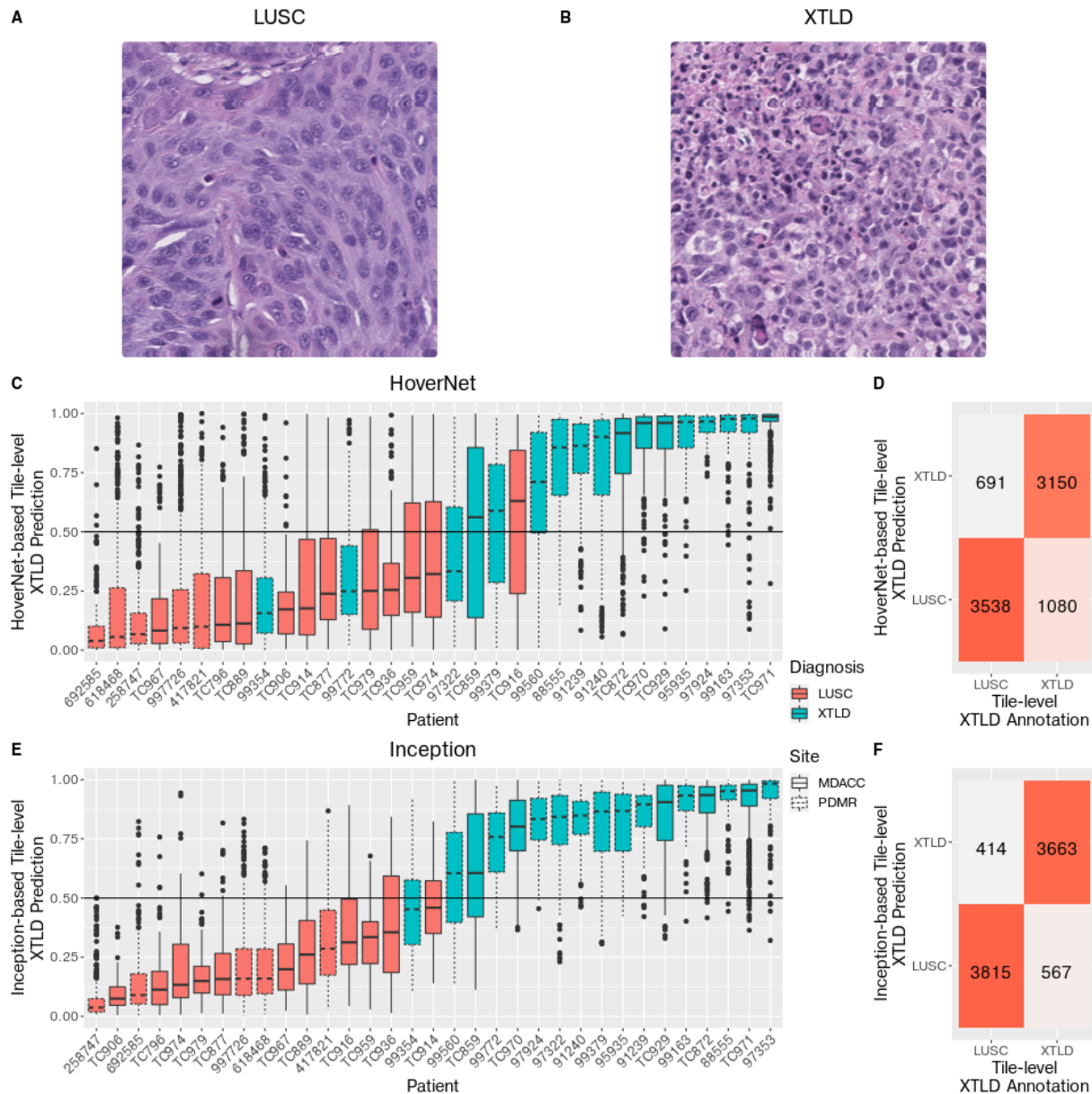


Fig 4. XTLD can be computationally predicted from H&E images using segmented and classified cells or deep learning features. (A, B) H&E images of (A) LUSC and (B) XTLD. (C, D) Hover-Net-based classifier performance. (C) Distribution of tile-level XTLD probability predicted by random forest trained using Hover-Net-derived features, according to patient (x axis) diagnoses with LUSC (red) or XTLD (blue) in the MDACC (solid line) or PDML (dashed line) datasets. Results shown for held-out set following 5-fold cross validation. (D) Confusion matrix showing tile-level concordance between Hover-Net-based classification (rows) and annotation (columns). (E, F) Inception-based classifier performance, as in (C, D), respectively, but with predictions from a random forest trained using Inception features.

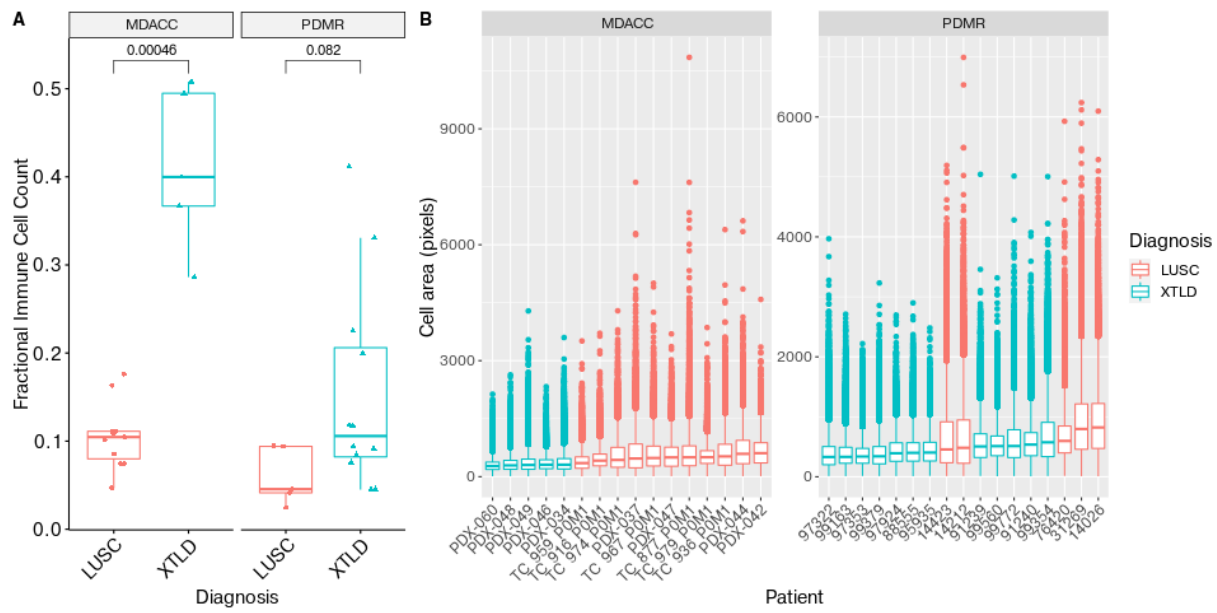


Fig S4. XTLD models have higher immune cell proportion and smaller cell size than LUSC models. (A) Proportion of immune cells relative to all segmented cells (y axis) in LUSC models (red) and XTLD models (blue) within MDACC and PDMR datasets. (B) Distribution of cell area (in pixels; y axis) across LUSC (red) and XTLD (blue) samples (x axis) in MDACC and PDMR datasets.

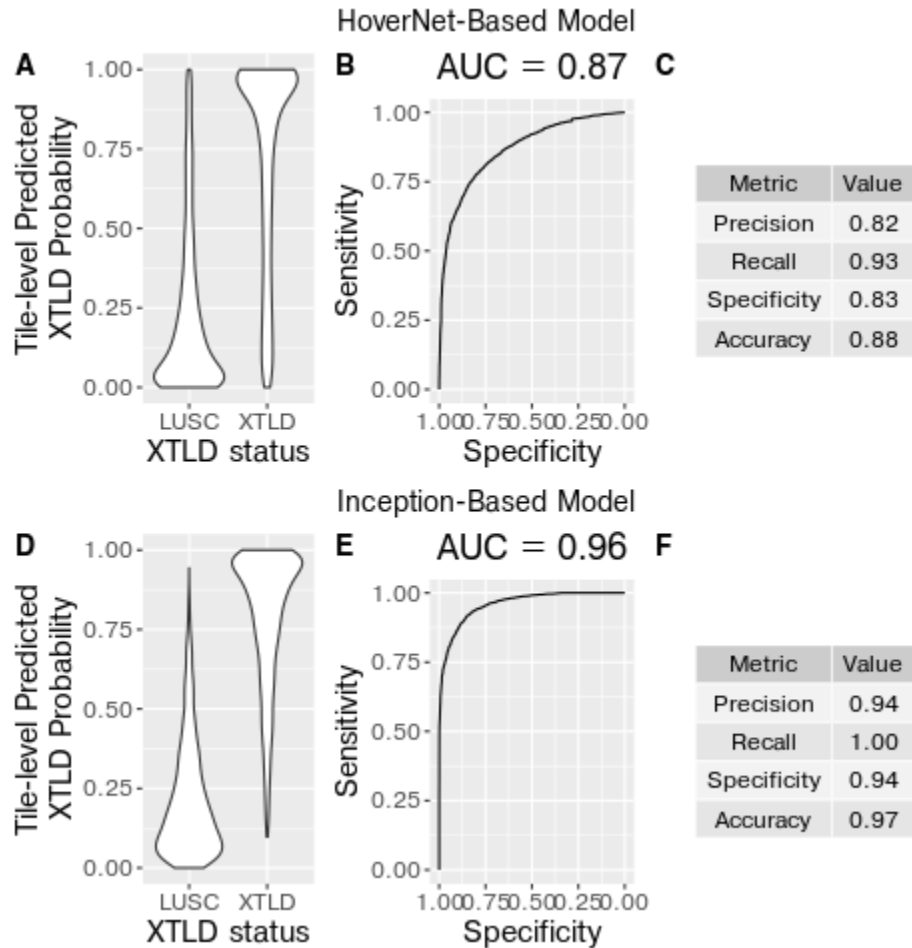


Fig S5. Inception-based classifier outperforms Hover-Net-based classifier in predicting XTLD. Performance of (A, B, C) Hover-Net-based and (D, E, F) Inception-based random forest classifiers of XTLD status. (A, D) Distribution of XTLD probability over tiles in images annotated as LUSC or XTLD as predicted by random forest trained on (A) Hover-Net or (B) Inception features. (B, E) AUC curves over tiles predicted (B) Hover-Net-based or (E) Inception-based classifier. (C, F) Tile-level performance metrics for (C) Hover-Net-based or (F) Inception-based classifier.

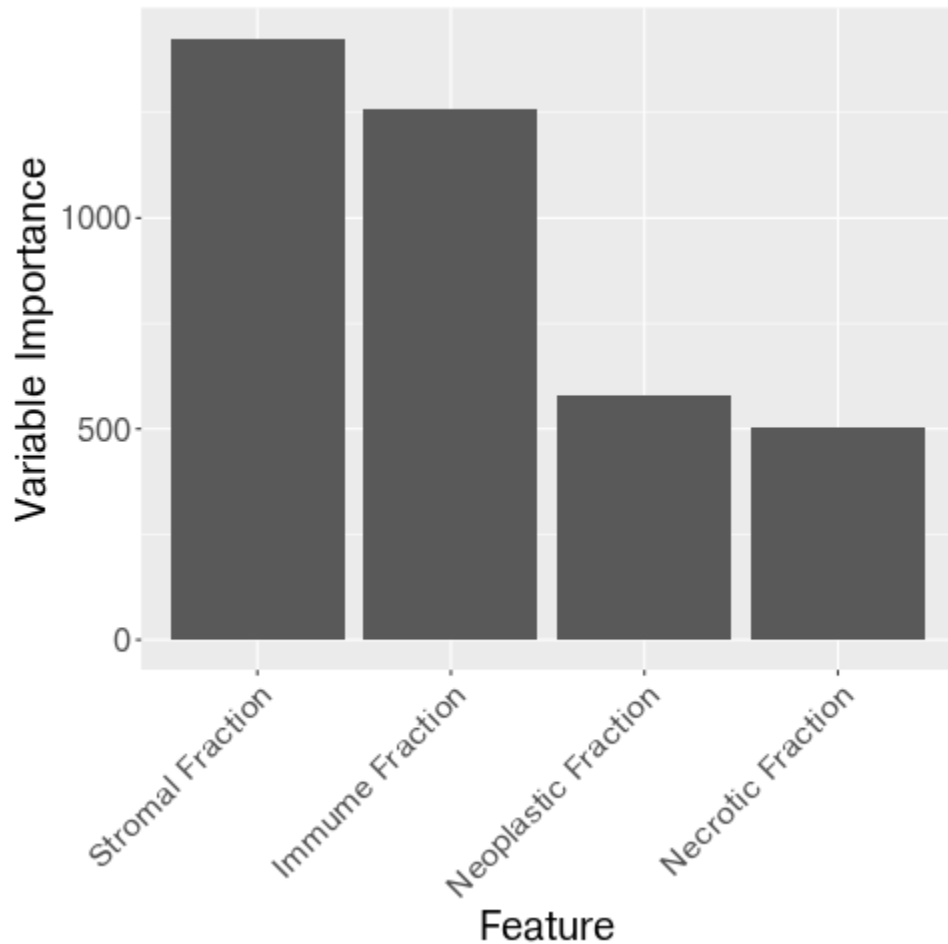


Fig S6. Stromal and immune proportions are more important than neoplastic and necrotic cell proportions in predicting XTLD. Variable importance of Hover-Net-based random forest classifier over tiles represented by proportion of segmented stromal, immune, neoplastic, and necrotic cells.

To interpret the information encoded by Inception that drives classification performance (Foroughi Pour et al. 2022), we examined feature 1895, the feature with highest variable importance in the random forest model (**Fig. S7**). We observed that this single feature segregated tiles in XTLD cases (high feature value) from those in LUSC cases (low feature value; **Fig. 5B**). A montage of tiles suggest that feature 1895 encodes cellular density and/or cell size (or something correlated with these) – those with high feature 1895 value (**Fig. 5C**) are dense in (small, round) lymphocytes or necrotic regions, while those with low value (**Fig. 5D**) have fewer, large cells and admixed stroma.

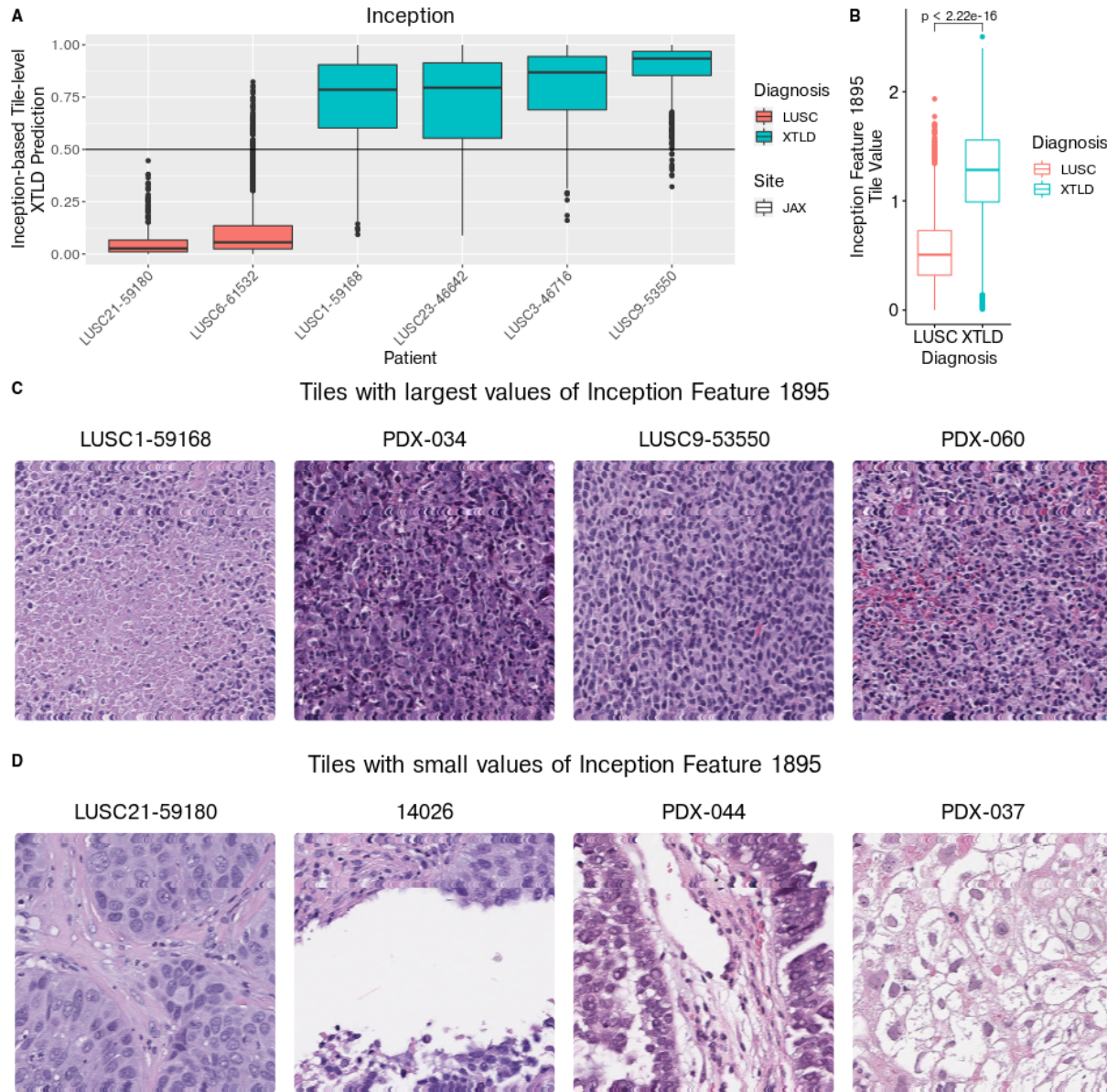


Fig 5. Inception encodes morphological features useful in predicting XTLD. (A) Distribution of tile-level XTLD probability predicted by random forest trained using Inception features, according to patient (x axis) diagnoses with LUSC (red) or XTLD (blue) in The Jackson Laboratory (JAX) external validation dataset. (B) Distribution of most important Inception feature (1895) across tiles within LUSC (red) or XTLD (blue) images. (C) Tiles with large values of Inception feature 1895. The tile with largest value is shown for each of four samples (noted above tile) with highest values, all of which are XTLD cases. (D) Tiles with small values of Inception feature 1895. The tile with smallest value is shown for each of four samples (noted above tile) with smallest values, all of which are LUSC cases.

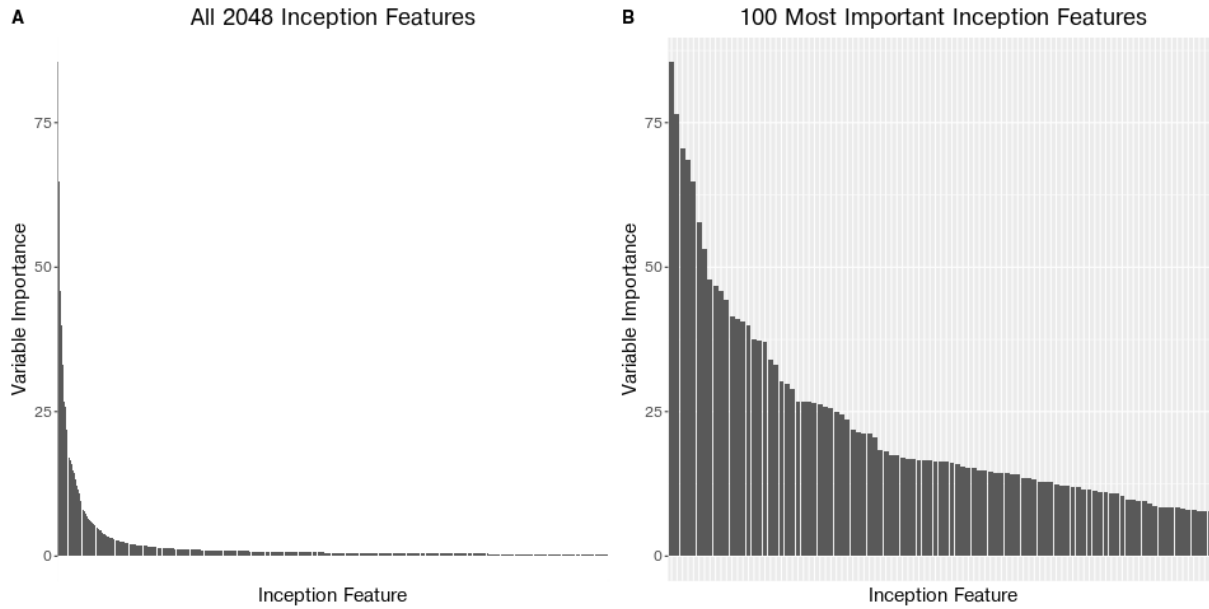


Fig S7. A small proportion of Inception features are important in classifying XTLD.
Variable importance of Inception-based random forest classifier for (A) all Inception features and (B) the top 100 Inception features.

Discussion

We presented a repository of nearly 1,000 H&E images of PDX samples and their human progenitors. All images are clinically annotated, many have paired expression and genomic data, and several have associated tumor, stromal, necrosis regions manually segmented by an expert pathologist. To the best of our knowledge, this is the first, large-scale, publicly-accessible set of PDX-derived images. As a demonstration of the utility of this resource, we provided two use cases: (1) a tumor-associated region classifier and (2) a classifier of XTLD – the unintended outgrowth of human lymphocytes, rather than the epithelial tumor cells, at the xenograft implantation site.

The images and all associated transcriptomic and genomic data, metadata, and annotations are hosted on the Seven Bridges Cancer Genomics Cloud [CGC; www.cancerogenomicscloud.org; (Lau et al. 2017)]. The CGC colocalizes data and computational resources, including those with graphics processing units (GPUs), in the cloud to enable efficient analysis. We have implemented the major components of our processing pipeline, namely quality control and tissue mask generation with HistoQC and cell segmentation and calling with Hover-Net, as publicly-available “apps” – effectively containers that can be automatically distributed across computational cloud resources for parallel processing of images. All analysis and processing for this manuscript was performed on the CGC. Practical execution of Hover-Net benefited from the

CGC, as it is computationally intensive and requires GPUs. By the time of publication, the images will also be hosted on the Imaging Data Commons (Fedorov et al. 2021) and all genomic and transcriptomic data are hosted on the PDXNet portal (Koc et al. 2022).

The repository enables exploration of several key biological questions, many specifically relevant to PDXs: (1) What morphological features of human tumors are recapitulated in PDXs? (2) Stromal cells and cancer-associated fibroblasts (CAFs), in particular, have been implicated in disease largely through their (highly varied) mediation of tumor / immune cell interactions (Mao et al. 2021). Do they retain this or some other function in immunocompromised mice? How are answers to these impacted by passaging, with early passages still harboring human immune and stromal cells and with murine CAFs replacing their human counterpart over time and passages (Blomme et al. 2018). Addressing these would be facilitated by placing immune and stromal cells in the context of the tumor core, periphery, or exterior using our regional classifier. (3) Automated grading of prostate (Nir et al. 2019), breast (Ehteshami Bejnordi et al. 2018), and colon (Vuong et al. 2020) cancers can be achieved through deep learning-based analysis of H&E images. Is tumor severity similarly imprinted on PDX sample morphology? If so, it should be possible to use the H&E images in our repository to predict their associated tumor stage and/or grade annotations. (4) Chemotherapy-treated breast samples exhibit morphological differences relative to treatment naive samples, including enlarged tumor cell nuclei (Rasbridge et al. 1994). Are such differences observed across tumor types and in PDX models? (5) Genetic mutations (Coudray et al. 2018) and gene expression (Schmauch et al. 2020) have been predicted from H&E using deep learning approaches. The (bulk) whole-exome sequencing and RNA-seq data paired with histology images in our repository would provide labels for transcriptome-wide studies in PDX samples. What gene mutations and expression patterns can be predicted? Do they validate published results (Coudray et al. 2018; Schmauch et al. 2020)? Are the associated, predictive morphological signatures preserved across tumor types?

Our region and XTLD classifiers were trained on features engineering from cells segmented and classified by one particular algorithm – Hover-Net. As a demonstration of the general applicability of our annotated images, we applied a second approach, Histology-based Digital (HD)-Staining, to a lung sample (S. Wang et al. 2020). HD-Staining has proven effective in classifying a rich set of cell types, including a tripartite separation of immune cells into macrophages, red blood cells, and a broader immune category. Intriguingly, we observed significant differences between Hover-Net- and HD-Staining-predicted cell types within stromal and necrotic regions annotated by our pathologist. These region-level annotations make possible a more systematic comparison of Hover-Net, HD-Staining, and related methods across other tumor types (Shmatko et al. 2022). This remains for future work.

H&E image color variability observed across institutions and labs (Nam et al. 2020; Otálora et al. 2019; Jose et al. 2021) may be caused by differences between stain batches and manufacturers, staining and fixation protocols, and tissue thickness (Veta et al. 2014; Bancroft 2008, chap. 10), as well as differences across imaging parameters, including scanner models (Leo et al. 2016) and image magnification (Komura and Ishikawa 2018). These site-specific effects adversely impact downstream DL-based classification (Shafiei et al. 2020; Salvi,

Michielli, and Molinari 2020; Zheng et al. 2019) and confound prediction of survival, mutations, and tumor stage (Howard et al. 2021). The resulting lack of generalizability is a significant barrier to clinical deployment of these approaches (van der Laak, Litjens, and Ciompi 2021). Several classes of color normalization attempt to address this issue: (1) template color matching maps summary statistics or histograms of RGB values in a reference image to those in a reference image (Reinhard et al. 2001; Kothari et al. 2011; Y.-Y. Wang et al. 2007; Magee et al. 2009; Janowczyk, Basavanhally, and Madabhushi 2017); (2) color deconvolution (Ruirok and Johnston 2001) represents each of the H&E dyes as a “stain vector” and substitutes a reference stain vector for the corresponding target vector (Macenko et al. 2009; Rabinovich, A. and Agarwal, S. and Laris, C. A. and Price, J. H. and Belongie, S. n.d.; Trahearn et al. 2015; Magee et al. 2009; Khan et al. 2014; Shafiei et al. 2020; Salvi, Michielli, and Molinari 2020; Zheng et al. 2019; Vahadane et al. 2016); and (3) generative adversarial network (GAN) approaches transfer stain distributions from a reference dataset (rather than single image) to a target dataset (Bentaieb and Hamarneh 2018; Tarek Shaban et al. 2018; Wagner et al. 2021). Our repository has considerable variability across the dimensions impacting image color, with six sites contributing data generated at two resolutions (20X and 40X) from different scanner models across multiple years. As such, it offers ample opportunity to compare color normalization approaches.

The H&E images presented here, alongside their genomic, transcriptomic, clinical, and pathological data, complement existing large-scale repositories, including TCGA, TCIA (Prior et al. 2013), GTEx (GTEx Consortium 2013), and CAMELYON17 (Litjens et al. 2018; Ehteshami Bejnordi et al. 2017; Bandi et al. 2019), while uniquely contributing PDX samples. As such, they expand the heterogeneity of publicly-accessible histology data available for technical studies (e.g., color normalization and batch correction), while also enabling exploration of the phenotypic effect of cellular interactions and morphology within a model system specifically intended to capture them.

Methods

Mapping imaging and genomic data. Images and genomic data are identified at the patient, model, and sample level. These levels are mapped using the following columns in the imaging and sequencing metadata for PDMR:

Imaging and sequencing mapping for PDMR data

	Patient	Model	Sample
Imaging Metadata Column	Patient.ID	Model.ID	Sample.ID
Sequencing Metadata Column	patient_id	specimen_id	pdmr_sample_id

Levels are mapped in the PDTCs using the following translations:

Imaging and sequencing mapping for PDTC data

	Patient	Model	Sample
Imaging Metadata Column	Patient.ID	Model.ID	Sample.ID
Sequencing Metadata Column	patient_id	model_id	sample_id

Image processing. For H&E images analyzed with Hover-Net or Inception, quality control and tissue segmentation were first performed using HistoQC (Janowczyk et al. 2019). Cell nuclei were then segmented and labeled as neoplastic, necrotic, immune, stromal, or other using Hover-Net (Graham et al. 2019). Features of 512 x 512 pixel tiles at 20X resolution (0.50 um per pixel) were computed using the Inception V3 convolutional neural network pre-trained on ImageNet (“Rethinking the Inception Architecture for Computer Vision” n.d.), as previously described (Noorbakhsh et al. 2020).

For H&E images analyzed with HD-Staining, tissue segmentation was first performed using Otsu thresholding followed with morphological dilation and erosions (Wang et al, 2018 <https://www.nature.com/articles/s41598-018-27707-4>). For whole slide analysis at 20X resolution, a 256 x 256 pixel window was slid over the entire tissue area with step size 226 pixel. Cell nuclei were then simultaneously segmented and classified as tumor, stroma, lymphocyte, red blood cell, macrophage, and karyorrhexis using HD-Staining (Wang et al, 2020). Only the nuclei with centroids located within the central 226 x 226 pixel area were kept to minimize the edge effect.

Predictive analyses. Regional and XTLD random forest classifiers were trained and evaluated using five-fold cross validation with the ranger R package (Wright and Ziegler 2017).

Funding

National Institutes of Health [NCI U24-CA224067, NCI U54-CA224083, NCI U54-CA224070, NCI U54-CA224065, NCI U54-CA224076, NCI U54-CA233223, NCI U54-CA233306]; National Cancer Institute; National Institutes of Health [HHSN261201400008C, HHSN261201500003I].

Conflict of interest statement. The University of Utah may choose to license PDX models developed in the Welm labs, which may result in tangible property royalties to Dr Welm and members of their lab who developed the models. Michael T. Lewis is a founder and limited partner in StemMed Ltd. and a manager in StemMed Holdings, its general partner. He is a founder and equity stake holder in Tvardi Therapeutics Inc. Some PDX are exclusively licensed

to StemMed Ltd. resulting in royalty income to MTL. Lacey Dobrolecki is a compensated employee of StemMed Ltd. The other authors declare no competing interest.

References

- Aeffner, Famke, Mark D. Zarella, Nathan Buchbinder, Marilyn M. Bui, Matthew R. Goodman, Douglas J. Hartman, Giovanni M. Lujan, et al. 2019. "Introduction to Digital Image Analysis in Whole-Slide Imaging: A White Paper from the Digital Pathology Association." *Journal of Pathology Informatics* 10 (March): 9.
- Bancroft, John D. 2008. *Theory and Practice of Histological Techniques*. Elsevier Health Sciences.
- Bandi, Peter, Oscar Geessink, Quirine Manson, Marcory Van Dijk, Maschenka Balkenhol, Meyke Hermsen, Babak Ehteshami Bejnordi, et al. 2019. "From Detection of Individual Metastases to Classification of Lymph Node Status at the Patient Level: The CAMELYON17 Challenge." *IEEE Transactions on Medical Imaging* 38 (2): 550–60.
- Ben-David, Uri, Gavin Ha, Yuen-Yi Tseng, Noah F. Greenwald, Coyin Oh, Juliann Shih, James M. McFarland, et al. 2017. "Patient-Derived Xenografts Undergo Mouse-Specific Tumor Evolution." *Nature Genetics* 49 (11): 1567–75.
- Bentaieb, Aicha, and Ghassan Hamarneh. 2018. "Adversarial Stain Transfer for Histopathology Image Analysis." *IEEE Transactions on Medical Imaging* 37 (3): 792–802.
- Bera, Kaustav, Kurt A. Schalper, David L. Rimm, Vamsidhar Velcheti, and Anant Madabhushi. 2019. "Artificial Intelligence in Digital Pathology - New Tools for Diagnosis and Precision Oncology." *Nature Reviews Clinical Oncology* 16 (11): 703–15.
- Blomme, Arnaud, Gaetan Van Simaeys, Gilles Doumont, Brunella Costanza, Justine Bellier, Yukihiro Otaka, Félicie Sherer, et al. 2018. "Murine Stroma Adopts a Human-like Metabolic Phenotype in the PDX Model of Colorectal Cancer and Liver Metastases." *Oncogene* 37 (9): 1237–50.
- Bondarenko, Gennadiy, Andrey Ugolkov, Stephen Rohan, Piotr Kulesza, Oleksii Dubrovskyi, Demirkan Gursel, Jeremy Mathews, Thomas V. O'Halloran, Jian J. Wei, and Andrew P. Mazar. 2015. "Patient-Derived Tumor Xenografts Are Susceptible to Formation of Human Lymphocytic Tumors." *Neoplasia* 17 (9): 735–41.
- Butler, Kristina A., Xiaonan Hou, Marc A. Becker, Valentina Zanfagnin, Sergio Enderica-Gonzalez, Daniel Visscher, Kimberly R. Kalli, Piyawan Tienchaianada, Paul Haluska, and S. John Weroha. 2017. "Prevention of Human Lymphoproliferative Tumor Formation in Ovarian Cancer Patient-Derived Xenografts." *Neoplasia* 19 (8): 628–36.
- Choi, Yoon Young, Jae Eun Lee, Hyunki Kim, Moon Hee Sim, Ka-Kyung Kim, Gunho Lee, Hyoung-II Kim, et al. 2016. "Establishment and Characterisation of Patient-Derived Xenografts as Paraclinical Models for Gastric Cancer." *Scientific Reports* 6 (March): 22172.
- Conklin, Matthew W., and Patricia J. Keely. 2012. "Why the Stroma Matters in Breast Cancer: Insights into Breast Cancer Patient Outcomes through the Examination of Stromal Biomarkers." *Cell Adhesion & Migration* 6 (3): 249–60.
- Coudray, Nicolas, Paolo Santiago Ocampo, Theodore Sakellaropoulos, Navneet Narula, Matija Snuderl, David Fenyö, Andre L. Moreira, Narges Razavian, and Aristotelis Tsirigos. 2018. "Classification and Mutation Prediction from Non-Small Cell Lung Cancer Histopathology Images Using Deep Learning." *Nature Medicine* 24 (10): 1559–67.
- Criscitiello, Carmen, Angela Esposito, and Giuseppe Curigliano. 2014. "Tumor-Stroma Crosstalk: Targeting Stroma in Breast Cancer." *Current Opinion in Oncology* 26 (6): 551–

55.

- Dieter, Sebastian M., Klara M. Giessler, Mark Kriegsmann, Taronish D. Dubash, Lino Möhrmann, Erik R. Schulz, Christine Siegl, et al. 2017. "Patient-Derived Xenografts of Gastrointestinal Cancers Are Susceptible to Rapid and Delayed B-Lymphoproliferation." *International Journal of Cancer. Journal International Du Cancer* 140 (6): 1356–63.
- Ehteshami Bejnordi, Babak, Maeve Mullooly, Ruth M. Pfeiffer, Shaoqi Fan, Pamela M. Vacek, Donald L. Weaver, Sally Herschorn, et al. 2018. "Using Deep Convolutional Neural Networks to Identify and Classify Tumor-Associated Stroma in Diagnostic Breast Biopsies." *Modern Pathology: An Official Journal of the United States and Canadian Academy of Pathology, Inc* 31 (10): 1502–12.
- Ehteshami Bejnordi, Babak, Mitko Veta, Paul Johannes van Diest, Bram van Ginneken, Nico Karssemeijer, Geert Litjens, Jeroen A. W. M. van der Laak, et al. 2017. "Diagnostic Assessment of Deep Learning Algorithms for Detection of Lymph Node Metastases in Women With Breast Cancer." *JAMA: The Journal of the American Medical Association* 318 (22): 2199–2210.
- Farahmand, Saman, Aileen I. Fernandez, Fahad Shabbir Ahmed, David L. Rimm, Jeffrey H. Chuang, Emily Reisenbichler, and Kourosh Zarringhalam. 2022. "Deep Learning Trained on Hematoxylin and Eosin Tumor Region of Interest Predicts HER2 Status and Trastuzumab Treatment Response in HER2+ Breast Cancer." *Modern Pathology: An Official Journal of the United States and Canadian Academy of Pathology, Inc* 35 (1): 44–51.
- Farmer, Pierre, Hervé Bonnefoi, Pascale Anderle, David Cameron, Pratyaksha Wirapati, Véronique Becette, Sylvie André, et al. 2009. "A Stroma-Related Gene Signature Predicts Resistance to Neoadjuvant Chemotherapy in Breast Cancer." *Nature Medicine* 15 (1): 68–74.
- Fedorov, Andrey, William J. R. Longabaugh, David Pot, David A. Clunie, Steve Pieper, Hugo J. W. L. Aerts, André Homeyer, et al. 2021. "NCI Imaging Data Commons." *Cancer Research* 81 (16): 4188–93.
- Foroughi Pour, Ali, Brian S. White, Jonghanne Park, Todd B. Sheridan, and Jeffrey H. Chuang. 2022. "Deep Learning Features Encode Interpretable Morphologies within Histological Images." *Scientific Reports* 12 (1): 9428.
- Graham, Simon, Quoc Dang Vu, Shan E. Ahmed Raza, Ayesha Azam, Yee Wah Tsang, Jin Tae Kwak, and Nasir Rajpoot. 2019. "Hover-Net: Simultaneous Segmentation and Classification of Nuclei in Multi-Tissue Histology Images." *Medical Image Analysis* 58 (December): 101563.
- Gray, Danny R., Wendy J. Huss, Jeffrey M. Yau, Lori E. Durham, Eric S. Werdin, William K. Funkhouser Jr, and Gary J. Smith. 2004. "Short-Term Human Prostate Primary Xenografts: An in Vivo Model of Human Prostate Cancer Vasculature and Angiogenesis." *Cancer Research* 64 (5): 1712–21.
- GTEx Consortium. 2013. "The Genotype-Tissue Expression (GTEx) Project." *Nature Genetics* 45 (6): 580–85.
- Howard, Frederick M., James Dolezal, Sara Kochanny, Jefree Schulte, Heather Chen, Lara Heij, Dezheng Huo, et al. 2021. "The Impact of Site-Specific Digital Histology Signatures on Deep Learning Model Accuracy and Bias." *Nature Communications* 12 (1): 4423.
- Janowczyk, Andrew, Ajay Basavanhally, and Anant Madabhushi. 2017. "Stain Normalization Using Sparse AutoEncoders (StaNoSA): Application to Digital Pathology." *Computerized Medical Imaging and Graphics: The Official Journal of the Computerized Medical Imaging Society* 57 (April): 50–61.
- Janowczyk, Andrew, Ren Zuo, Hannah Gilmore, Michael Feldman, and Anant Madabhushi. 2019. "HistoQC: An Open-Source Quality Control Tool for Digital Pathology Slides." *JCO Clinical Cancer Informatics* 3 (April): 1–7.
- Johannet, Paul, Nicolas Coudray, Douglas M. Donnelly, George Jour, Irineu Illa-Bochaca, Yuhe

- Xia, Douglas B. Johnson, et al. 2021. "Using Machine Learning Algorithms to Predict Immunotherapy Response in Patients with Advanced Melanoma." *Clinical Cancer Research: An Official Journal of the American Association for Cancer Research* 27 (1): 131–40.
- Jose, Laya, Sidong Liu, Carlo Russo, Annemarie Nadort, and Antonio Di Ieva. 2021. "Generative Adversarial Networks in Digital Pathology and Histopathological Image Processing: A Review." *Journal of Pathology Informatics* 12 (November): 43.
- Kather, Jakob Nikolas, Johannes Krisam, Pornpimol Charoentong, Tom Luedde, Esther Herpel, Cleo-Aron Weis, Timo Gaiser, et al. 2019. "Predicting Survival from Colorectal Cancer Histology Slides Using Deep Learning: A Retrospective Multicenter Study." *PLoS Medicine* 16 (1): e1002730.
- Khan, Adnan Mujahid, Nasir Rajpoot, Darren Treanor, and Derek Magee. 2014. "A Nonlinear Mapping Approach to Stain Normalization in Digital Histopathology Images Using Image-Specific Color Deconvolution." *IEEE Transactions on Bio-Medical Engineering* 61 (6): 1729–38.
- Koc, Soner, Michael W. Lloyd, Jeffrey W. Grover, Nan Xiao, Sara Seepo, Sai Lakshmi Subramanian, Manisha Ray, et al. 2022. "PDXNet Portal: Patient-Derived Xenograft Model, Data, Workflow and Tool Discovery." *NAR Cancer* 4 (2): zcac014.
- Komura, Daisuke, and Shumpei Ishikawa. 2018. "Machine Learning Methods for Histopathological Image Analysis." *Computational and Structural Biotechnology Journal* 16 (February): 34–42.
- Kothari, Sonal, John H. Phan, Richard A. Moffitt, Todd H. Stokes, Shelby E. Hassberger, Qaiser Chaudry, Andrew N. Young, and May D. Wang. 2011. "Automatic Batch-Invariant Color Segmentation of Histological Cancer Images." *Proceedings / IEEE International Symposium on Biomedical Imaging: From Nano to Macro. IEEE International Symposium on Biomedical Imaging 2011* (March): 657–60.
- Laak, Jeroen van der, Geert Litjens, and Francesco Ciompi. 2021. "Deep Learning in Histopathology: The Path to the Clinic." *Nature Medicine* 27 (5): 775–84.
- Lau, Jessica W., Erik Lehnert, Anurag Sethi, Raunaq Malhotra, Gaurav Kaushik, Zeynep Onder, Nick Groves-Kirkby, et al. 2017. "The Cancer Genomics Cloud: Collaborative, Reproducible, and Democratized-A New Paradigm in Large-Scale Computational Research." *Cancer Research* 77 (21): e3–6.
- Leo, Patrick, George Lee, Natalie N. C. Shih, Robin Elliott, Michael D. Feldman, and Anant Madabhushi. 2016. "Evaluating Stability of Histomorphometric Features across Scanner and Staining Variations: Prostate Cancer Diagnosis from Whole Slide Images." *Journal of Medical Imaging (Bellingham, Wash.)* 3 (4): 047502.
- Li, Junjie, Weiming Mi, Yucheng Guo, Xinyu Ren, Hao Fu, Tao Zhang, Hao Zou, and Zhiyong Liang. 2022. "Artificial Intelligence for Histological Subtype Classification of Breast Cancer: Combining Multi-Scale Feature Maps and the Recurrent Attention Model." *Histopathology* 80 (5): 836–46.
- Li, Shunqiang, Dong Shen, Jieya Shao, Robert Crowder, Wenbin Liu, Aleix Prat, Xiaping He, et al. 2013. "Endocrine-Therapy-Resistant ESR1 Variants Revealed by Genomic Characterization of Breast-Cancer-Derived Xenografts." *Cell Reports* 4 (6): 1116–30.
- Litjens, Geert, Peter Bandi, Babak Ehteshami Bejnordi, Oscar Geessink, Maschenka Balkenhol, Peter Bult, Altuna Halilovic, et al. 2018. "1399 H&E-Stained Sentinel Lymph Node Sections of Breast Cancer Patients: The CAMELYON Dataset." *GigaScience* 7 (6). <https://doi.org/10.1093/gigascience/giy065>.
- Macenko, Marc, Marc Niethammer, J. S. Marron, David Borland, John T. Woosley, Xiaojun Guan, Charles Schmitt, and Nancy E. Thomas. 2009. "A Method for Normalizing Histology Slides for Quantitative Analysis." In *2009 IEEE International Symposium on Biomedical Imaging: From Nano to Macro*. IEEE. <https://doi.org/10.1109/isbi.2009.5193250>.

- Magee, D., D. Treanor, D. Crellin, M. Shires, Katherine J. E. Smith, K. Mohee, and P. Quirke. 2009. "Colour Normalisation in Digital Histopathology Images." In *Proc Optical Tissue Image Analysis in Microscopy, Histopathology and Endoscopy (MICCAI Workshop)*. <https://www.semanticscholar.org/paper/Colour-Normalisation-in-Digital-Histopathology-Magee-Treanor/8efdf7bc5e765673feae964735a9ebd1312e8b99>.
- Mao, Xiaoqi, Jin Xu, Wei Wang, Chen Liang, Jie Hua, Jiang Liu, Bo Zhang, Qingcai Meng, Xianjun Yu, and Si Shi. 2021. "Crosstalk between Cancer-Associated Fibroblasts and Immune Cells in the Tumor Microenvironment: New Findings and Future Perspectives." *Molecular Cancer* 20 (1): 131.
- Nam, Soojeong, Yosep Chong, Chan Kwon Jung, Tae-Yeong Kwak, Ji Youl Lee, Jihwan Park, Mi Jung Rho, and Heounjeong Go. 2020. "Introduction to Digital Pathology and Computer-Aided Pathology." *Journal of Pathology and Translational Medicine* 54 (2): 125–34.
- Nir, Guy, Davood Karimi, S. Larry Goldenberg, Ladan Fazli, Brian F. Skinnider, Peyman Tavassoli, Dmitry Turbin, et al. 2019. "Comparison of Artificial Intelligence Techniques to Evaluate Performance of a Classifier for Automatic Grading of Prostate Cancer From Digitized Histopathologic Images." *JAMA Network Open* 2 (3): e190442.
- Noorbakhsh, Javad, Saman Farahmand, Ali Foroughi Pour, Sandeep Namburi, Dennis Caruana, David Rimm, Mohammad Soltanieh-Ha, Kourosh Zarringhalam, and Jeffrey H. Chuang. 2020. "Deep Learning-Based Cross-Classifications Reveal Conserved Spatial Behaviors within Tumor Histological Images." *Nature Communications* 11 (1): 6367.
- Otalora, Sebastian, Manfredo Atzori, Vincent Andrearczyk, Amjad Khan, and Henning Müller. 2019. "Staining Invariant Features for Improving Generalization of Deep Convolutional Neural Networks in Computational Pathology." *Frontiers in Bioengineering and Biotechnology* 7 (August): 198.
- Petrillo, Laura A., Denise M. Wolf, Ann M. Kapoun, Nicholas J. Wang, Andrea Barczak, Yuanyuan Xiao, Hasan Korkaya, et al. 2012. "Xenografts Faithfully Recapitulate Breast Cancer-Specific Gene Expression Patterns of Parent Primary Breast Tumors." *Breast Cancer Research and Treatment* 135 (3): 913–22.
- Plava, Jana, Marina Cihova, Monika Burikova, Miroslava Matuskova, Lucia Kucerova, and Svetlana Miklikova. 2019. "Recent Advances in Understanding Tumor Stroma-Mediated Chemoresistance in Breast Cancer." *Molecular Cancer* 18 (1): 67.
- Pompili, Luca, Manuela Porru, Carla Caruso, Annamaria Biroccio, and Carlo Leonetti. 2016. "Patient-Derived Xenografts: A Relevant Preclinical Model for Drug Development." *Journal of Experimental & Clinical Cancer Research: CR* 35 (1): 189.
- Prior, Fred W., Ken Clark, Paul Commean, John Freymann, Carl Jaffe, Justin Kirby, Stephen Moore, et al. 2013. "TCIA: An Information Resource to Enable Open Science." *Conference Proceedings: ... Annual International Conference of the IEEE Engineering in Medicine and Biology Society. IEEE Engineering in Medicine and Biology Society. Conference* 2013: 1282–85.
- Rabinovich, A. and Agarwal, S. and Laris, C. A. and Price, J. H. and Belongie, S. n.d. "Unsupervised Color Decomposition of Histologically Stained Tissue Samples." In *NIPS'03: Proceedings of the 16th International Conference on Neural Information Processing Systems*. Accessed September 29, 2022. <https://dl.acm.org/doi/10.5555/2981345.2981429>.
- Rasbridge, S. A., C. E. Gillett, A. M. Seymour, K. Patel, M. A. Richards, R. D. Rubens, and R. R. Millis. 1994. "The Effects of Chemotherapy on Morphology, Cellular Proliferation, Apoptosis and Oncoprotein Expression in Primary Breast Carcinoma." *British Journal of Cancer* 70 (2): 335–41.
- Rawat, Rishi R., Itzel Ortega, Preeyam Roy, Fei Sha, Darryl Shibata, Daniel Ruderman, and David B. Agus. 2020. "Deep Learned Tissue 'Fingerprints' Classify Breast Cancers by ER/PR/Her2 Status from H&E Images." *Scientific Reports* 10 (1): 7275.
- Reinhard, E., M. Adhikhmin, B. Gooch, and P. Shirley. 2001. "Color Transfer between Images."

- IEEE Computer Graphics and Applications* 21 (4): 34–41.
- “Rethinking the Inception Architecture for Computer Vision.” n.d. Accessed October 18, 2022. <https://doi.org/10.1109/cvpr.2016.308>.
- Ruifrok, A. C., and D. A. Johnston. 2001. “Quantification of Histochemical Staining by Color Deconvolution.” *Analytical and Quantitative Cytology and Histology / the International Academy of Cytology [and] American Society of Cytology* 23 (4): 291–99.
- Saltz, Joel, Rajarsi Gupta, Le Hou, Tahsin Kurc, Pankaj Singh, Vu Nguyen, Dimitris Samaras, et al. 2018. “Spatial Organization and Molecular Correlation of Tumor-Infiltrating Lymphocytes Using Deep Learning on Pathology Images.” *Cell Reports* 23 (1): 181–93.e7.
- Salvi, Massimo, Nicola Michielli, and Filippo Molinari. 2020. “Stain Color Adaptive Normalization (SCAN) Algorithm: Separation and Standardization of Histological Stains in Digital Pathology.” *Computer Methods and Programs in Biomedicine* 193 (September): 105506.
- Sanz, Laura, Angel M. Cuesta, Clara Salas, César Corbacho, Carmen Bellas, and Luís Alvarez-Vallina. 2009. “Differential Transplantability of Human Endothelial Cells in Colorectal Cancer and Renal Cell Carcinoma Primary Xenografts.” *Laboratory Investigation; a Journal of Technical Methods and Pathology* 89 (1): 91–97.
- Schmauch, Benoît, Alberto Romagnoni, Elodie Pronier, Charlie Saillard, Pascale Maillé, Julien Calderaro, Aurélie Kamoun, et al. 2020. “A Deep Learning Model to Predict RNA-Seq Expression of Tumours from Whole Slide Images.” *Nature Communications* 11 (1): 3877.
- Shafiei, Sobhan, Amir Safarpoor, Ahd Jamalizadeh, and H. R. Tizhoosh. 2020. “Class-Agnostic Weighted Normalization of Staining in Histopathology Images Using a Spatially Constrained Mixture Model.” *IEEE Transactions on Medical Imaging* 39 (11): 3355–66.
- Shmatko, Artem, Narmin Ghaffari Laleh, Moritz Gerstung, and Jakob Nikolas Kather. 2022. “Artificial Intelligence in Histopathology: Enhancing Cancer Research and Clinical Oncology.” *Nature Cancer* 3 (9): 1026–38.
- Sirinukunwattana, Korsuk, Enric Domingo, Susan D. Richman, Keara L. Redmond, Andrew Blake, Clare Verrill, Simon J. Leedham, et al. 2021. “Image-Based Consensus Molecular Subtype (imCMS) Classification of Colorectal Cancer Using Deep Learning.” *Gut* 70 (3): 544–54.
- Srinidhi, Chetan L., Ozan Ciga, and Anne L. Martel. 2021. “Deep Neural Network Models for Computational Histopathology: A Survey.” *Medical Image Analysis* 67 (January): 101813.
- Szegedy, Christian, Vincent Vanhoucke, Sergey Ioffe, Jon Shlens, and Zbigniew Wojna. 2016. “Rethinking the Inception Architecture for Computer Vision.” In *2016 IEEE Conference on Computer Vision and Pattern Recognition (CVPR)*. IEEE. <https://doi.org/10.1109/cvpr.2016.308>.
- Tarek Shaban, M., Christoph Baur, Nassir Navab, and Shadi Albarqouni. 2018. “StainGAN: Stain Style Transfer for Digital Histological Images.” *arXiv [cs.CV]*. arXiv. <http://arxiv.org/abs/1804.01601>.
- Tentler, John J., Aik Choon Tan, Colin D. Weekes, Antonio Jimeno, Stephen Leong, Todd M. Pitts, John J. Arcaroli, Wells A. Messersmith, and S. Gail Eckhardt. 2012. “Patient-Derived Tumour Xenografts as Models for Oncology Drug Development.” *Nature Reviews. Clinical Oncology* 9 (6): 338–50.
- “The Impact of Tumor Stroma on Drug Response in Breast Cancer.” 2015. *Seminars in Cancer Biology* 31 (April): 3–15.
- Trahearn, Nicholas, David Snead, Ian Cree, and Nasir Rajpoot. 2015. “Multi-Class Stain Separation Using Independent Component Analysis.” In *Medical Imaging 2015: Digital Pathology*, 9420:113–23. SPIE.
- Tran, Khoa A., Olga Kondrashova, Andrew Bradley, Elizabeth D. Williams, John V. Pearson, and Nicola Waddell. 2021. “Deep Learning in Cancer Diagnosis, Prognosis and Treatment Selection.” *Genome Medicine* 13 (1): 152.
- Vahadane, Abhishek, Tingying Peng, Amit Sethi, Shadi Albarqouni, Lichao Wang, Maximilian

- Baust, Katja Steiger, Anna Melissa Schlitter, Irene Esposito, and Nassir Navab. 2016. "Structure-Preserving Color Normalization and Sparse Stain Separation for Histological Images." *IEEE Transactions on Medical Imaging* 35 (8): 1962–71.
- Veta, Mitko, Josien P. W. Pluim, Paul J. van Diest, and Max A. Viergever. 2014. "Breast Cancer Histopathology Image Analysis: A Review." *IEEE Transactions on Bio-Medical Engineering* 61 (5): 1400–1411.
- Vuong, Thi Le Trinh, Daigeun Lee, Jin Tae Kwak, and Kyungeun Kim. 2020. "Multi-Task Deep Learning for Colon Cancer Grading." In *2020 International Conference on Electronics, Information, and Communication (ICEIC)*. IEEE. <https://doi.org/10.1109/iceic49074.2020.9051305>.
- Wagner, Sophia J., Nadieh Khalili, Raghav Sharma, Melanie Boxberg, Carsten Marr, Walter de Back, and Tingying Peng. 2021. "Structure-Preserving Multi-Domain Stain Color Augmentation Using Style-Transfer with Disentangled Representations." *arXiv [eess.IV]*. arXiv. <http://arxiv.org/abs/2107.12357>.
- Wang, Shidan, Ruichen Rong, Donghan M. Yang, Junya Fujimoto, Shirley Yan, Ling Cai, Lin Yang, et al. 2020. "Computational Staining of Pathology Images to Study the Tumor Microenvironment in Lung Cancer." *Cancer Research*.
- Wang, Yi-Ying, Shao-Chien Chang, Li-Wha Wu, Sen-Tien Tsai, and Yung-Nien Sun. 2007. "A Color-Based Approach for Automated Segmentation in Tumor Tissue Classification." *Conference Proceedings: ... Annual International Conference of the IEEE Engineering in Medicine and Biology Society. IEEE Engineering in Medicine and Biology Society. Conference 2007*: 6577–80.
- Woo, Xing Yi, Jessica Giordano, Anuj Srivastava, Zi-Ming Zhao, Michael W. Lloyd, Roebi de Brujin, Yun-Suhk Suh, et al. 2021. "Conservation of Copy Number Profiles during Engraftment and Passaging of Patient-Derived Cancer Xenografts." *Nature Genetics* 53 (1): 86–99.
- Woo, Xing Yi, Anuj Srivastava, Joel H. Gruber, Vinod Yadav, Vishal Kumar Sarsani, Al Simons, Glen Beane, et al. 2019. "Genomic Data Analysis Workflows for Tumors from Patient-Derived Xenografts (PDXs): Challenges and Guidelines." *BMC Medical Genomics* 12 (1): 92.
- Wright, Marvin N., and Andreas Ziegler. 2017. "Ranger: A Fast Implementation of Random Forests for High Dimensional Data in C++ and R." *Journal of Statistical Software* 77 (1). <https://doi.org/10.18637/jss.v077.i01>.
- Zhang, Lianhai, Yiqiang Liu, Xiaohong Wang, Zhiyu Tang, Shuangxi Li, Ying Hu, Xianglong Zong, et al. 2015. "The Extent of Inflammatory Infiltration in Primary Cancer Tissues Is Associated with Lymphomagenesis in Immunodeficient Mice." *Scientific Reports* 5 (March): 9447.
- Zhang, Xiaomei, Sofie Claerhout, Aleix Prat, Lacey E. Dobrolecki, Ivana Petrovic, Qing Lai, Melissa D. Landis, et al. 2013. "A Renewable Tissue Resource of Phenotypically Stable, Biologically and Ethnically Diverse, Patient-Derived Human Breast Cancer Xenograft Models." *Cancer Research* 73 (15): 4885–97.
- Zheng, Yushan, Zhiguo Jiang, Haopeng Zhang, Fengying Xie, Jun Shi, and Chenghai Xue. 2019. "Adaptive Color Deconvolution for Histological WSI Normalization." *Computer Methods and Programs in Biomedicine* 170 (March): 107–20.